Materials Today: Proceedings 75 (2023) 16–22

Contents lists available at ScienceDirect

Materials Today: Proceedings

journal homepage: www.elsevier.com/locate/matpr

Geometry reconstruction for additive manufacturing: From G-CODE to 3D CAD model

Antonio Bacciaglia *, Francesco Falcetelli, Enrico Troiani, Raffaella Di Sante, Alfredo Liverani, Alessandro Ceruti

Department of Industrial Engineering, University of Bologna, 47121 Forlì, Italy

ARTICLE INFO

Article history:
Available online 5 October 2022

Keywords:
Additive Manufacturing
Fused Deposition Modelling
G-CODE
CAD

ABSTRACT

In the last decades, the flourishing of Additive Manufacturing (AM) promoted innovative design solutions in many different sectors. Despite the numerous advantages of AM technology, there are still open challenges in the field. In Fused Deposition Modelling (FDM) structures the layer-by-layer manufacturing process induces anisotropy in the material properties of the structures. The correct characterization of the mechanical properties is fundamental in the design and development stages but at the same time difficult to achieve. The experimental approach can be extremely long and expensive. An alternative is the use of an accurate numerical approach and performing a Finite Element Analysis (FEA) of the geometry which is effectively printed. However, to the best of the authors' knowledge, there is not a common and well-established procedure to reconstruct the real geometry which is generated after the slicing process. In this paper, starting from the information provided by the G-CODE, an easy-to-use, and reproducible methodology to reconstruct the printed geometry is presented. The performance of the innovative approach is evaluated via qualitative observations by referring to several case studies. The results are thoroughly analysed, and future trends and research needs are highlighted.

Selection and peer-review under responsibility of the scientific committee of the Innovative Manufacturing, Mechatronics & Material Forum 2022.

1. Introduction

In the last decades, Additive Manufacturing (AM) employment skyrocketed not only in industrial engineering contexts such as automotive [1], aerospace [2] and biomedical [3] but also in more exotic fields such as jewellery, clothing [4], and even in the manufacturing of musical instruments [5]. AM is viewed as a viable alternative to traditional manufacturing methods such as chip removal, casting, milling, and lathing, which all require adherence to many design limitations [6]. This manufacturing technology is based on the addition of new raw materials layer by layer, and it is extremely convenient for all those applications characterized by small, customized production volumes and for rapid prototyping of down-scaled models, mock-ups and so on [7]. AM technology has various benefits, including a quick design-to-manufacturing cycle, design flexibility, the capacity to create complicated forms in one piece, limiting the waste of raw material and the ability to mimic low-weight bioinspired geometries.

Nowadays the design tools available to engineers do not keep up with the constant innovations of AM technologies [8] and the strong limits of Computer-aided design (CAD) software in the integration of design, technology, optimization, and smoothing processes highlighted in the literature [9]. In addition, the key drawbacks of AM technology to date are the material anisotropic qualities and the high surface roughness, especially valid for the Fused Deposition Modelling (FDM) technique [10] investigated in this research. Furthermore, AM is characterized by a restricted material portfolio; inspection and maintenance in complicated one-piece assemblies are problematic. High raw material and machine prices, and a delayed certification procedure affect AM products. This is owing to the substantial structural performance variability caused by differences in raw material qualities, changes (often minor) in machine settings or ambient factors, and the response of AM structures under fatigue loads.

In the typical design workflow, especially for critical applications, after the 3D digital model is designed, engineers should

* Corresponding author.
E-mail address: antonio.bacciaglia2@unibo.it (A. Bacciaglia).

https://doi.org/10.1016/j.matpr.2022.09.496
2214-7853/
Selection and peer-review under responsibility of the scientific committee of the Innovative Manufacturing, Mechatronics & Material Forum 2022.

investigate the mechanical behaviour of manufactured components through numerical or experimental approaches before the commercialization of the final product. On the one hand, in the scientific literature is plenty of contributions dealing with the description and discussion of experimental tests of AM specimens (FDM [11], Stereolithography [12] and Selective Laser Melting [13;14]) while few contributions employ Finite Element Analysis (FEA) to estimate the mechanical performances even if it is well known that FEA has an extremely lower economic impact on a typical design workflow. Indeed, several material configurations and manufacturing settings can be rapidly tested without wasting raw material and the operator's working hours.

However, the strong anisotropy, i.e. a significant change in mechanical characteristics in various directions, of AM products [15] limits the diffusion of numerical approaches in the literature. Thus, due to the inherent anisotropy, complex components, and unpredictable quality of 3D-printed components, traditional methods of FEA may not be suitable. If on the one hand FEA well estimates the behaviour of components created by traditional techniques, on the other, it cannot reliably forecast the behaviour of 3D-printed parts. Moreover, the multitude of Additive Manufacturing processes and the relatively new technology still in a development phase, hence rather few strength data, add to the complexity. Researchers established many assumptions to simulate the mechanical characteristics of AM objects through simplified models.

Though, the approximations are confined to certain load scenarios or AM processes. For example, [16] focuses just on tensile loads applied on FDM specimens and estimates their stiffness by applying the strength of materials principles. To evaluate the elastic properties of additive produced components under compressive stresses, [17] used the rule of mixture and property transformation equation and excellent agreement between analytical and experimental findings was discovered. Of particular interest are the study reported in [18], in which a layered sub-modelling technique and FEA were used to assess the mechanical properties of 3D-printed components and in [19] where a computational homogenization technique is used to get the mechanical behaviour of 3D printed composite laminates. This is the only contribution that seeks to explain mechanical behaviour by using the true geometry of additively created parts starting from tooling path information. The process for obtaining the rebuilt geometry, however, is not mentioned. Indeed, to get the 3D real geometry model for FEA purposes, reverse modelling techniques should be developed knowing the tooling path, i.e. extrusion head for FDM, contained in the G-CODE files. In this regard, [20] can be seen as a first step towards the mimic of the real geometry for optical fibers embedding [21] in AM products using a manual reconstruction coded in Python, taking inspiration from the resulting preview of G-CODEs in slicing software.

Thus, to the best of the authors' knowledge, there is a lack of contributions dealing with the reconstruction of the real geometry from the tooling path information with a clear and reproducible methodology. From the analysis of the state-of-the-art [22], it has been highlighted the need for ease and reproducible methodologies capable of reconstructing the real 3D geometry from the information collected in the G-CODEs file useful for FEA. Currently, to simulate the mechanical properties of 3Dprinted objects, simplified models are used. However, these approaches are not capable of modelling the anisotropic nature of AM parts. Thus, tools and solvers should be created to accurately estimate and characterise the mechanical characteristics to use FEA to approximate the behaviour of additively manufactured objects.

To overcome this technological gap, this research aims to describe a never-explored reproducible methodology which aim is to extract and obtain the 3D real geometry model of AM products, suitable for FEAs. This is done starting from the reading of useful information contained in the G-CODE which is used to recreate the tool path of AM machines. A set of simple geometries with variable infill and printing settings is used to validate the approaches and to compare the performances of the programmed routines through qualitative analysis.

2. Methodology

The methodology developed in this research aims to generate a STEP file representing the real printed geometry as output given a certain G-CODE as input. The STEP format enables comprehensive product specifications to be exchanged between CAD and FEM environments. To reconstruct the true geometry coming from the FDM process, the authors propose to exploit the capabilities offered by the sweep command, available in every CAD package. Indeed, using the sweep command, a 2D object (profile) is swept along an open or closed route (spine) to generate a 3D surface or solid. The sweep command specification is ideal for the suggested methodology's goal of reconstructing real-world produced geometry: with the extrusion section profile and the route of the extruder's tool, any form may be recreated.

The final aim of the research is achieved through three main steps, represented by the three coloured blocks in Fig. 1. In the following subsections, each block is explained in detail.

2.1. Coordinates extraction from G-CODE

The G-CODE file is generated using common slicing software. For the scope of this research, the open-source software Ultimaker Cura [23] has been employed. The initial objective is to extract the information about the toolpath coordinates included in the G-GODE, once it is accessible. Indeed, the scope is to track the lines where there is material extrusion and nozzle movement since there is no interest in tracking lines with feed rate or extrusion temperature changes. This task is achieved using the following steps:

- read the G-CODE file as a series of strings of characters;
- the lines of interest are identified by reading the keyword at the front of each stringer line. In particular, three keywords are of interest for the scope of the research, namely the G0 and G1 commands (extrusion head motion) and the LAYER command, meaning a change of the extruded layer;

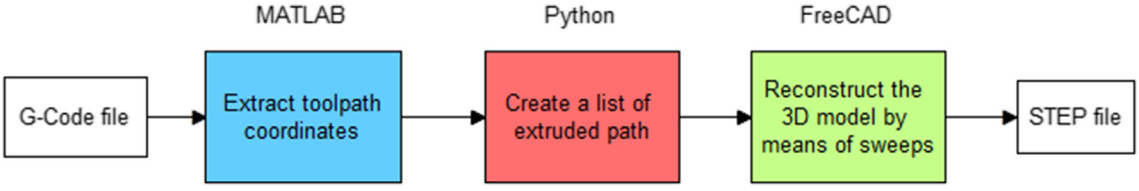

Fig. 1. Main methodology flow chart.

- depending on the command contained in each line, a flag is assigned:
  - flag = 1 if the instruction contains an extrusion command (G1);
  - flag = 2 if the instruction contains an extrusion head movement without extruded material (G0);
  - flag = 3 if the instruction contains a layer change (LAYER);
- for each of these lines, an array containing the spatial coordinates of the tooling path and the relative flag is saved;
- the final mx4 matrix is saved as.mat file.
- The procedure can be visually summarized by looking at the flow chart in Fig. 2.

2.2. Definition of the extruded path as a sweep list

Once the toolpath coordinates are available, a Python code has been developed to provide a list containing all the sweep paths (spines) to be generated. At this level, just the movements involving the material extrusion should be evaluated. It's vital to distinguish between situations when the nozzle is extruding material (flag = 1) and situations where the nozzle is just moving to a different coordinate without printing (flag = 2). This is done by exploiting the flag values available at two consecutive lines. Referring to Table 1, the flag couples in the "A" scenario correspond to the toolpath coordinates where extrusion is taking place, whereas if the flag couples lie in the "B" scenario, then the toolpath coordinates do not have to be considered for the sweep procedure. For example, if line i contains a LAYER command (flag = 3), and line i + 1 contains a G1 command (flag = 1), the FDM machine is deposing material from the starting point contained in i to the point i + 1 (first column in Table 1). On the other hand, if line i contains a G1 command (flag = 1) and i + 1 contains a G0 instruction (flag = 2), the tool is moving from point i to i + 1 without extruding new material (fourth column of Table 1) and for this reason, this case should not be considered in the sweep path reconstruction.

Whenever Case A is encountered, the new point is added to the open list, while if Case B appears at some point, it means that the continuous extrusion of material is interrupted by an extrusion head movement. For this reason, the actual list containing the coordinates of a sweep spine should be closed and a new list can be created. A list containing all the spine paths, considered as lists, can be exported as a.csv file. The complete flowchart of this procedure is shown in Fig. 3.

2.3. FreeCAD 3D model reconstruction

The last step leverages the open-source software FreeCAD to make all the sweep commands by reading the.csv file produced in the previous step. To adapt the methodology to different case studies, the user can choose between three different sweep profiles. For simplification purposes, circular and rectangular profiles could be adopted, while the 'slot' one, somehow approximates the real nozzle profile (Fig. 4). For example, the rectangular profile could be used to obtain a final geometry with sharp corners where a structured mesh could be adopted in an FEA, whereas the slot profile could be used to better reproduce the final geometry and model the actual bonding between different layers. Once all the sweep operations are completed, the FreeCAD macro exports a STEP file containing the real printed geometry. Fig. 5 summarizes this methodology in a flowchart.

3. Results

3.1. Computational time evaluation

The performance of the code is assessed by measuring the computational time needed for different case studies to recreate the

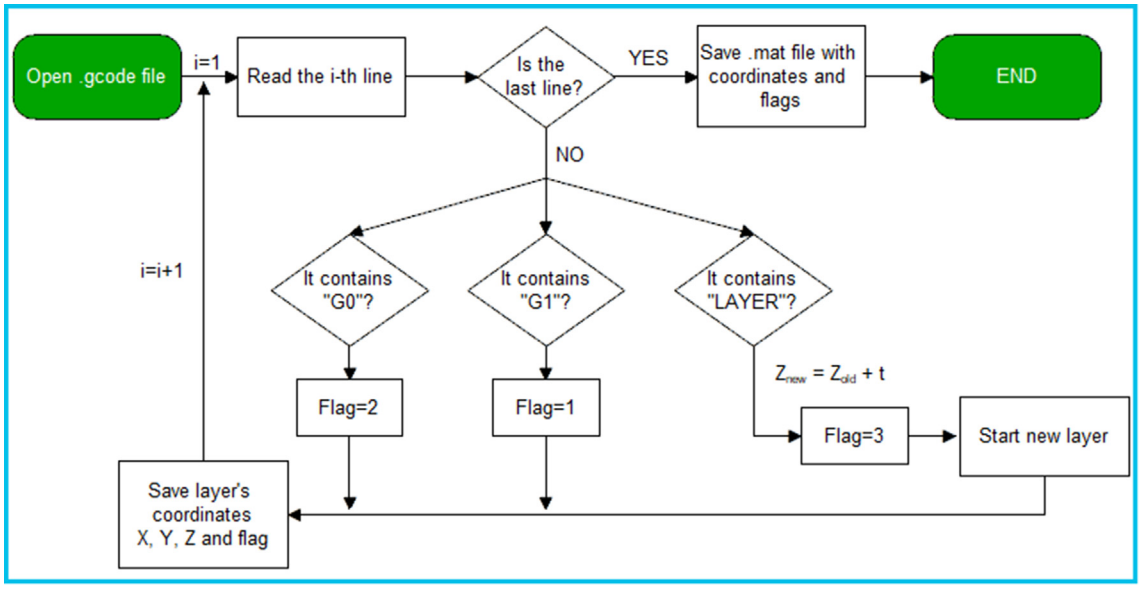

Fig. 2. Flow chart of the G-CODE extraction algorithm.

Table 1
Definition of two possible scenarios (A and B) based on flag values of two consecutive G-CODE lines.

	A			B				
i^{th} Line	3	1	2	1	2	2	1	3
$(i + 1)^{th}$ Line	1	1	1	2	2	3	3	2

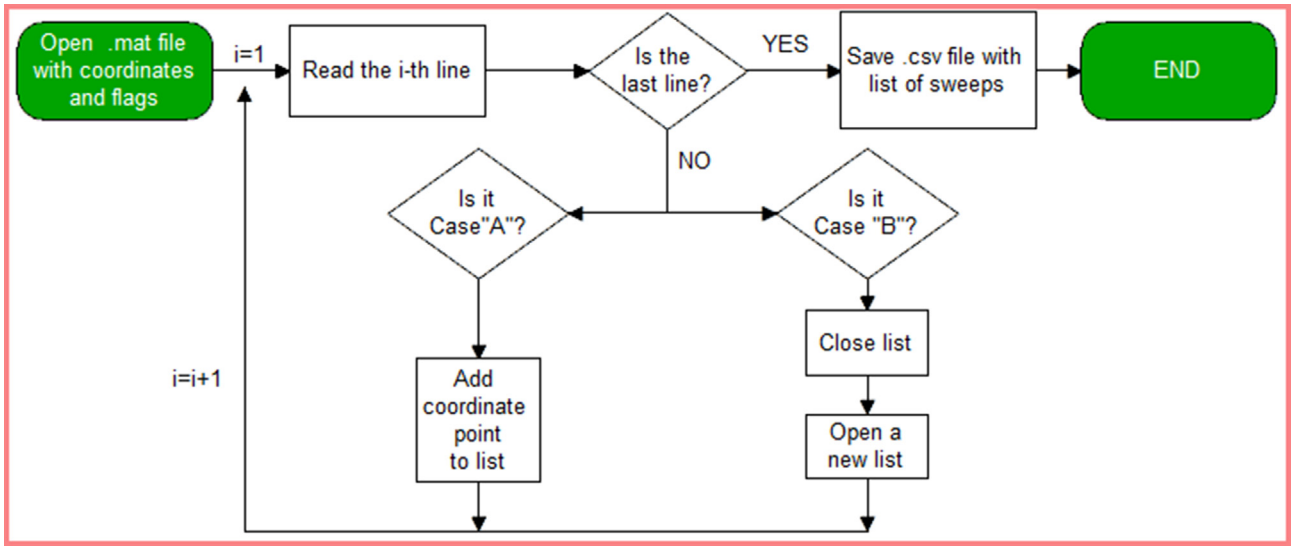

Fig. 3. Sweep list management through python code.

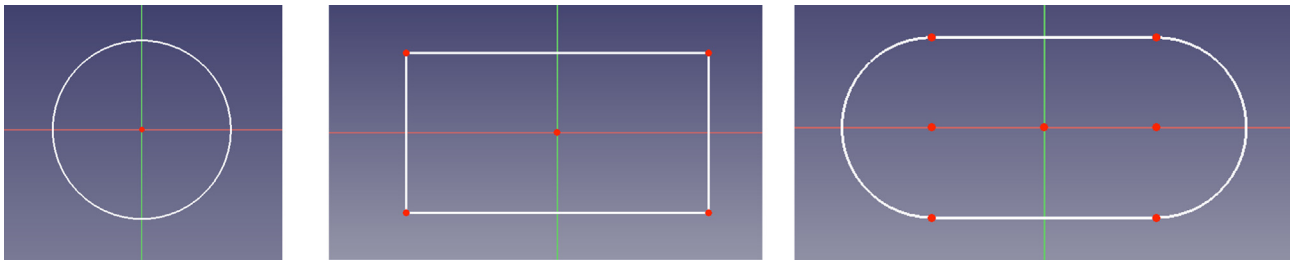

Fig. 4. Implemented sweep profiles library: circular (left), rectangular (centre) and slot (right).

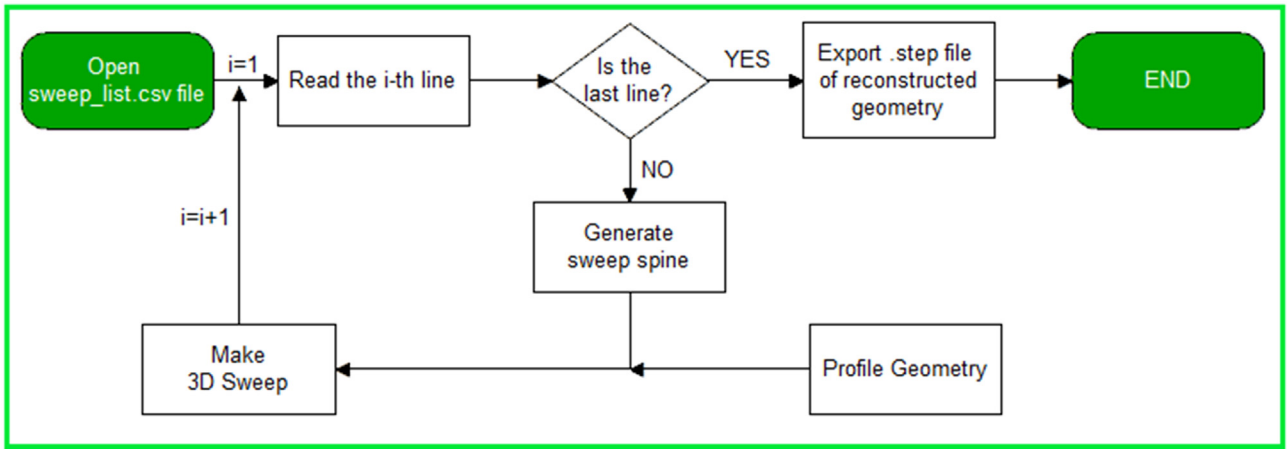

Fig. 5. FreeCAD flowchart for real geometry reconstruction.

actual geometry. All the simulations are performed by running the programmed codes on a workstation with 128 GB RAM and an Intel i9-11900 @ 2.50 GHz CPU. Two geometries are considered: a cube with dimensions of 10 × 10 × 10 mm and a 30 × 100 mm dog-bone specimen. The dog-bone model has been used to test the methodology in a real case scenario and to highlight the capability of the innovative approach to model even curved paths rather than straight ones. Then, for each shape, different infill percentages and profile topologies are tested to see how these parameters affect the approach's efficiency. The gyroid and pyramid infill types, in particular, have been used to see how the methodology behaves with a gradient in the infill pattern along the third direction. Finally, each of these cases is further divided into three additional subcases corresponding to the three different geometry profiles. This comprehensive collection of simulations allows the reader to see how the infill pattern and density, the exterior geometry, and the profile used, affect the methodology performance.

The results are outlined in Table 2. The times' columns were coloured according to a conditional formatting rule: the more a certain time value is lower than the mean of the three profiles time

Table 2
The computational time for different case studies.

	Infill		Sweeps	Time [s]			G-CODE	
Cases	[%]	Type	no	Circular	Rectangular	Slot	KB	No Lines
Cube 10 × 10 × 10	20	Lines	443	73.00	68.80	87.50	64	2430
Cube 10 × 10 × 10	50	Lines	827	376.40	361.30	379.50	104	4014
Cube 10 × 10 × 10	100	Lines	1499	1478.60	1419.30	1449.70	122	4062
Dog-bone specimen	10	Lines	1069	720.90	693.00	740.90	192	6726
Dog-bone specimen	20	Lines	1621	1742.90	1666.80	1682.00	248	8804
Dog-bone specimen	50	Lines	3231	7889.10	7705.10	7508.40	401	14,436
Dog-bone specimen	100	Lines	5899	62384.10	60815.30	63944.40	487	15,490
Cube 10 × 10 × 10	20	Gyroid	375	110.00	78.60	106.70	220	7404
Dog-bone specimen	20	Pyramid	1578	1571.60	1540.00	1560.00	231	8020

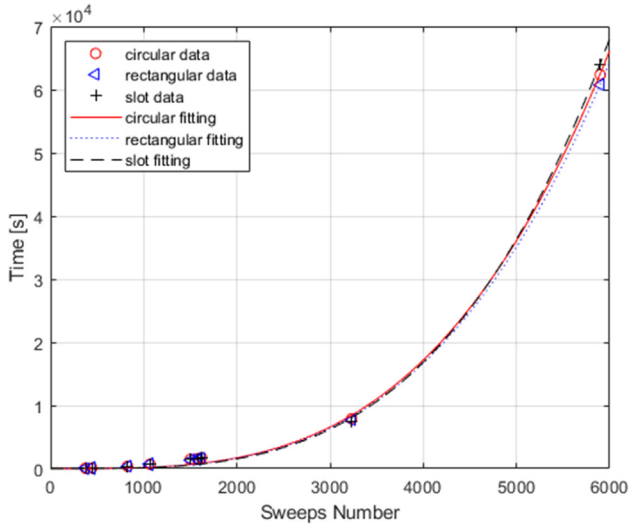

Fig. 6. Computational time versus the number of sweeps for different sweep profiles and 3D models.

values, being fixed the infill % and the digital model, the more its colour tends to be green. In the opposite case, the cell value tends toward the red colour. It is visible at a glance that the rectangular profile is the most efficient while, depending on the specific cases, the circular or the slot profiles require more time.

Moreover, it is possible to infer that the computational time depends on the number of sweeps rather than on the G-CODE file dimension as one may expect.

The data contained in Table 2 are plotted and fitted using the MATLAB fitting toolbox, which highlighted that a power law exists between the number of sweeps and the numerical simulation time (Fig. 6).

3.2. Quality assessment of reconstructed geometry

The quality of the reconstructed geometry was assessed with several qualitative observations of the tested case studies. For instance, Fig. 7 shows how the dog-bone specimen geometry (20% infill) was reconstructed. From a first evaluation, it is possible to say that all the main geometry features were correctly captured and reconstructed, such as the outer skin and the infill type.

The three-section views shown in Fig. 8 prove that the proposed code was able to reconstruct the real printed cube geometry using the three different sweep profiles.

The last qualitative observation has been made considering as a case study the cube with the gyroid infill type, because of its complex topology made of curved paths and not constant along with different layers. The cube was printed using an Artillery Sidewinder X1 FDM machine. The printing process was deliberately interrupted before completion to show the gyroid infill pattern (Fig. 9 left). This result is compared with the one obtained in the FreeCAD reconstruction process (Fig. 9 right). The results suggest that the methodology was reliable even in the case of a complex infill pattern.

4. Discussion and conclusions

This study investigates a new and reproducible methodology to reconstruct the geometry of additively manufactured components knowing the G-CODE information. The reconstructed shape is exported as a STEP file to make it compatible with the majority

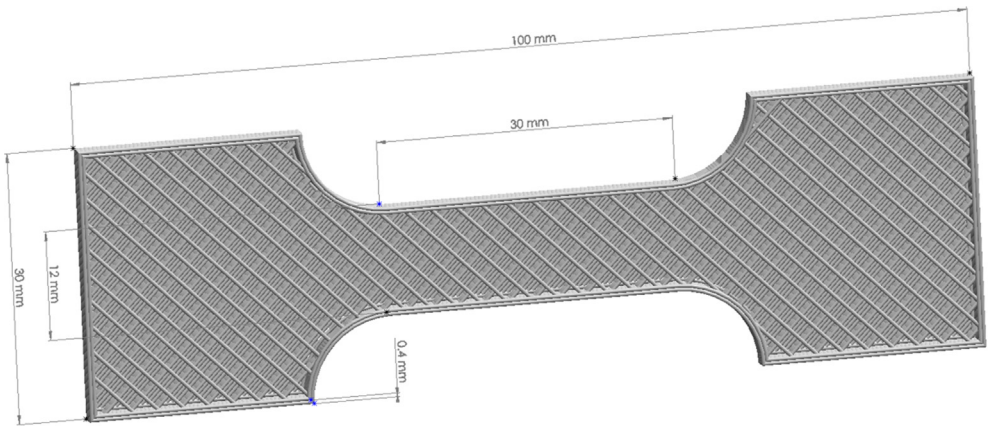

Fig. 7. Example of geometry reconstruction of a specimen with a 20% infill.

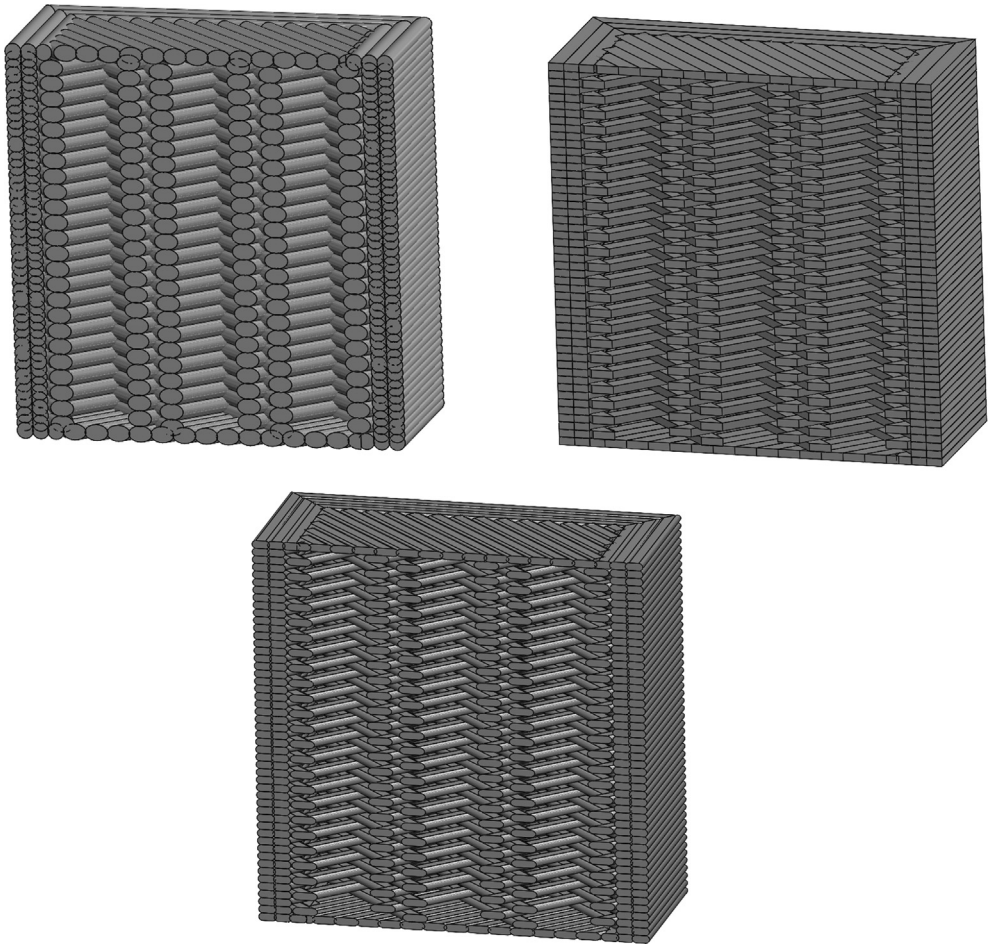

Fig. 8. Profiles comparison: circular (up-left), rectangular (up-right), and slot (down-centre) with highlighted edges for a more comprehensive geometry visualization.

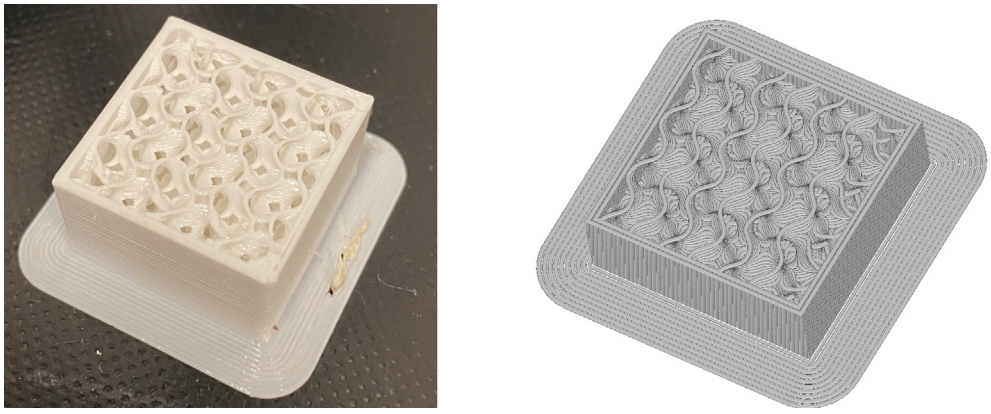

Fig. 9. Comparison of real geometry (left), and reconstructed geometry in FreeCAD (right).

of CAD and FEM packages. The aim of the research is achieved in three main steps namely: toolpath coordinates extraction (MATLAB), filtering of Marlin instructions and creation of a list of extrusion paths to be reproduced (Python), and geometry reconstruction through sweeps (FreeCAD). Table 3 summarizes the pros and cons of the proposed methodology.

Different geometries, infill patterns and density and sweep profiles are qualitatively investigated to understand their effect on the methodology performance. The results proved to be promising in

Table 3
Advantages and challenges of the methodology.

Pros	Cons
Possibility to reconstruct different profile sections and infills	Limited profile section portfolio
External geometry does not affect the methodology	Limited by computational requirements
Ease and reproducible	1st version includes three different software

terms of reconstruction quality even in the most complex scenarios. At the same time, the computational time might be a limiting factor for the simulation of bigger components because it grows with a power law as a function of the number of sweeps to be generated. In this regard, assuming that the astonishing increase in computational power seen in the last decade will continue at the same rate, it is reasonable to assume that bigger and more complex geometry, which now are unfeasible to reconstruct, might be modelled with this approach in the near future. Then, this potentially opens the possibility of importing the STEP file into an FEA software for structural simulations without requiring expensive and time-consuming experimental campaigns.

The technique will be evaluated on additional topologies with a larger range of infill patterns and density in future research. To evaluate the importing, management, and meshing of complex 3D models, the final geometry will be uploaded into FEA software. Thus, a numerical technique might be utilised to comprehend the component's mechanical behaviour and compare it to experimental data to determine the validity of the approach presented in this study. Furthermore, the proposed methodology paves the way for the development of models specifically addressing the intra and inter-layer bounding of the material, where the anisotropy can be modelled by adjusting the amount of overlapping region within adjacent layers.

To conclude, this work aims to provide a practical guide to all the researchers involved in the modelling of AM components in a clear and reproducible manner. We hope that this paper could promote and foster in the scientific community the need of sharing a common methodology to model AM structures.

CRediT authorship contribution statement

Antonio Bacciaglia: Conceptualization, Methodology, Software, Data curation, Writing – original draft. **Francesco Falcetelli:** Conceptualization, Methodology, Software, Data curation, Writing – original draft. **Enrico Troiani:** Resources. **Raffaella Di Sante:** Supervision. **Alfredo Liverani:** Project administration. **Alessandro Ceruti:** Writing – review & editing.

Declaration of Competing Interest

The authors declare that they have no known competing financial interests or personal relationships that could have appeared to influence the work reported in this paper.

References

[1] S. Mantovani, S.G. Barbieri, M. Giacopini, A. Croce, A. Sola, E. Bassoli, Synergy between topology optimization and additive manufacturing in the automotive field, Proc. Institut. Mech. Engineers, Part B: J. Eng. Manuf. 235 (3) (2021) 555–567.

[2] L. Zhu, N. Li, P.R.N. Childs, Light-weighting in aerospace component and system design, Propul. Power Res. 7 (2) (2018) 103–119, https://doi.org/10.1016/j.jppr.2018.04.001.

[3] H.S. Park, D.S. Nguyen, T. Le-Hong, X. Van Tran, Machine learning-based optimization of process parameters in selective laser melting for biomedical applications, J. Intell. Manuf. 33 (6) (2022) 1843–1858.

[4] T.D. Ngo, A. Kashani, G. Imbalzano, K.T.Q. Nguyen, D. Hui, Additive manufacturing (3D printing): A review of materials, methods, applications and challenges, Compos. B Eng. 143 (2018) 172–196, https://doi.org/10.1016/j.compositesb.2018.02.012.

[5] A. Bacciaglia, A. Ceruti, A. Liverani, Evaluation of 3D printed mouthpieces for musical instruments, RPJ 26 (3) (2019) 577–584, https://doi.org/10.1108/RPJ-07-2019-0187.

[6] I. Campbell, D. Bourell, I. Gibson, Additive manufacturing: rapid prototyping comes of age, Rapid Prototyp. J. 18 (4) (2012) 255–258, https://doi.org/10.1108/13552541211231563.

[7] I. Gibson, D.W. Rosen, B. Stucker, Additive manufacturing technologies: 3D printing, rapid prototyping, and direct digital manufacturing, 2. ed., Springer, New York, NY, 2015.

[8] G. Vega, R. Paz, A. Gleadall, M. Monzón, M.E. Alemán-Domínguez, Comparison of CAD and Voxel-Based Modelling Methodologies for the Mechanical Simulation of Extrusion-Based 3D Printed Scaffolds, Materials 14 (19) (2021) 5670, https://doi.org/10.3390/ma14195670.

[9] A. Bacciaglia, A. Ceruti, A. Liverani, Surface smoothing for topological optimized 3D models, Struct. Multidisc. Optim. 64 (6) (2021) 3453–3472.

[10] O.A. Mohamed, S.H. Masood, J.L. Bhowmik, Modeling, analysis, and optimization of dimensional accuracy of FDM-fabricated parts using definitive screening design and deep learning feedforward artificial neural network, Adv. Manuf. 9 (1) (2021) 115–129, https://doi.org/10.1007/s40436-020-00336-9.

[11] B. Rankouhi, S. Javadpour, F. Delfanian, T. Letcher, Failure Analysis and Mechanical Characterization of 3D Printed ABS With Respect to Layer Thickness and Orientation, J Fail. Anal. Prevent. 16 (3) (2016) 467–481, https://doi.org/10.1007/s11668-016-0113-2.

[12] J.M. Dulieu-Barton, M.C. Fulton, Mechanical Properties of a Typical Stereolithography Resin, Strain 36 (2) (2000) 81–87, https://doi.org/10.1111/j.1475-1305.2000.tb01177.x.

[13] S. Romano, A. Brückner-Foit, A. Brandão, J. Gumpinger, T. Ghidini, S. Beretta, Fatigue properties of AlSi10Mg obtained by additive manufacturing: Defect-based modelling and prediction of fatigue strength, Eng. Fract. Mech. 187 (2018) 165–189, https://doi.org/10.1016/j.engfracmech.2017.11.002.

[14] P. Mercelis, J. Kruth, Residual stresses in selective laser sintering and selective laser melting, Rapid Prototyp. J. 12 (5) (2006) 254–265, https://doi.org/10.1108/13552540610707013.

[15] C.S. Lee, S.G. Kim, H.J. Kim, S.H. Ahn, Measurement of anisotropic compressive strength of rapid prototyping parts, J. Mater. Process. Technol. 187–188 (2007) 627–630, https://doi.org/10.1016/j.jmatprotec.2006.11.095.

[16] J.F. Rodríguez, J.P. Thomas, J.E. Renaud, Mechanical behavior of acrylonitrile butadiene styrene fused deposition materials modeling, Rapid Prototyp. J. 9 (4) (2003) 219–230, https://doi.org/10.1108/13552540310489604.

[17] M. Sugavaneswaran, G. Arumaikkannu, Analytical and experimental investigation on elastic modulus of reinforced additive manufactured structure, Mater. Des. 66 (2015) 29–36.

[18] J. Zarbakhsh, A. Iravani, Z. Amin-Akhlaghi, Sub-modeling Finite Element Analysis of 3D printed structures, in: 2015 16th International Conference on Thermal, Mechanical and Multi-Physics Simulation and Experiments in Microelectronics and Microsystems, Budapest, Hungary, Apr. 2015, pp. 1–4. doi: 10.1109/EuroSimE.2015.7103095.

[19] M. Somireddy, A. Czekanski, Computational modeling of constitutive behaviour of 3D printed composite structures, J. Mater. Res. Technol. 11 (2021) 1710–1718, https://doi.org/10.1016/j.jmrt.2021.02.030.

[20] F. Falcetelli, R. Di Sante, E. Troiani, Strategies for Embedding Optical Fiber Sensors in Additive Manufacturing Structures, in: European Workshop on Structural Health Monitoring, vol. 128, P. Rizzo and A. Milazzo, Eds. Cham: Springer International Publishing, 2021, pp. 362–371. doi: 10.1007/978-3-030-64908-1_34.

[21] F. Falcetelli, L. Rossi, R. Di Sante, G. Bolognini, Strain Transfer in Surface-Bonded Optical Fiber Sensors, Sensors 20 (11) (2020) 3100, https://doi.org/10.3390/s20113100.

[22] J.R.C. Dizon, A.H. Espera, Q. Chen, R.C. Advincula, Mechanical characterization of 3D-printed polymers, Addit. Manuf. 20 (2018) 44–67, https://doi.org/10.1016/j.addma.2017.12.002.

[23] 'Ultimaker Cura'. Accessed: May 30, 2022. [Online]. Available: https://ultimaker.com/it/software.